

The intergrain exchange coupling in Sm(Co,Fe,Cu,Zr)_{*z*} magnets with *z* = 7.0 and 7.5

Ren-Jie Chen¹, Jin-Zhi Wang², Hong-Wei Zhang²,
Bao-Gen Shen² and Aru Yan¹

¹ Ningbo Institute of Materials Technology & Engineering, Chinese Academy of Sciences, Ningbo 315201, People's Republic of China

² State Key Laboratory of Magnetism, Institute of Physics and Centre for Condensed Matter Physics, Chinese Academy of Sciences, Beijing 100080, People's Republic of China

E-mail: chenrj@nimte.ac.cn

Received 11 April 2007, in final form 24 May 2007

Published 13 July 2007

Online at stacks.iop.org/JPhysD/40/4391

Abstract

The magnetic behaviour of Sm(Co,Fe,Cu,Zr)_{*z*} ribbons with *z* = 7.0 and 7.5 is investigated. The Henkel plots indicate that there is a strong intergrain exchange coupling (IGEC) effect in these ribbons. It is the IGEC that results in the phenomena of the interaction domains and remanence enhancement in the ribbons at room temperature. The contributions of IGEC and dipolar interaction to irreversible magnetization have been analysed to explain the phenomenon of open recoil loops. Due to the difference of the intensity of the IGEC, the magnetization changes with the component of the Sm(Co,Fe,Cu,Zr)_{*z*} ribbons.

1. Introduction

Sm-Co based permanent magnets (PMs) have attracted much attention since the 1990s because of the abnormal temperature dependence of coercivity H_c found in Sm(Co,Fe,Cu,Zr)_{*z*} alloys [1–4]. These kinds of magnets have been named high temperature magnets or modern Sm(Co,Fe,Cu,Zr)_{*z*} magnets with positive temperature coefficients of H_c in a certain temperature range [5, 6]. The experimental results indicate that these kinds of magnets have the same cellular microstructure as the traditional Sm(Co,Fe,Cu,Zr)_{*z*} magnets in which the value of H_c reduces rapidly with the increase temperature. The microstructure of precipitation-hardened Sm₂Co₁₇-based PMs consists of a 2 : 17 type cell (~ 100 nm) surrounded by a 1 : 5 type cell wall (~ 10 nm) [2–4, 7–9]. It is generally accepted that the coercivity mechanism of these precipitation-hardened magnets is controlled by the domain wall pinning due to the difference of domain wall energy density between two phases. Up to now, much attention has been paid to the modern Sm(Co,Fe,Cu,Zr)_{*z*} magnets to understand the mechanism of the abnormal temperature dependence of coercivity and to obtain high performance at high temperatures [2, 3, 5, 8, 10–12], while the effect of intergrain exchanging coupling (IGEC) on the magnetization process has hardly been noticed. Considering the ultrafine

microstructure, IGEC should play an important role in this cellular type PMs as observed in the nanocomposite PMs [13, 14].

In nanocomposite exchanging coupled magnets, such as melt-spun Nd₂Fe₁₄B-typed ribbons, the exchange coupling between magnetically hard and soft phases determines the magnetic moments of the soft phase to align with those of the hard phase resulting in the remanence enhancement for isotropic magnets. Therefore, a high $(BH)_{\max}$ could be obtained in exchange coupled magnets due to IGEC. Some interesting phenomena in many nanocomposite magnets have been observed, such as the high degree of reversibility in the demagnetization behaviour and the relatively open recoil loops [7, 13–15]. This indicates that IGEC visibly affects the demagnetization process in nanocomposite magnets. In this paper, IGEC has been studied in modern and traditional Sm(Co,Fe,Cu,Zr)_{*z*} ribbons by experimental investigations in terms of the magnetic domains structure, the magnetization and demagnetization processes at different temperatures.

2. Experiments

The alloys with a nominal composition of Sm(Co_{bal}Fe_{0.1}Cu_{0.1}Zr_{0.03})_{7.0} (sample A) and Sm(Co_{bal}Fe_{0.1}Cu_{0.1}Zr_{0.03})_{7.5}

(sample B) were prepared by arc melting under high purified argon gas atmosphere. The purity of the constituent elements is at least 99.9%. The ingots were remelted four times to achieve a good homogeneity. The ribbons were prepared by the melt-spinning technique. The Cu wheel surface velocity of 5 m s^{-1} has been used in this work. The ribbons were aged at 850°C for 3 h, followed by slow cooling at 1 K min^{-1} to 450°C , and then quenched to room temperature. The heat treatment is necessary to obtain the desired microstructure and microchemistry, and this results in the excellent magnetic property.

The magnetic measurements in the temperature range from room temperature (RT) to 700°C were performed using a high temperature LakeShore vibrating sample magnetometer (VSM) with a maximum field of 24 kOe. The demagnetization factor of the specimens has been neglected because the magnetic measurements were performed along the longitudinal direction of the ribbons. The structural analysis was carried out by x-ray diffraction (XRD) with Cu $\text{K}\alpha$ radiation, and the magnetic domain structure was studied using a Digital Instruments NanoScope IIIA D-3000 magnetic force microscope (MFM) at RT.

3. Results and discussion

Figure 1 shows the XRD patterns of the ribbons. Both $\text{Th}_2\text{Zn}_{17}$ and CaCu_5 structure phases are detected in the two ribbons. But the diffraction peaks of the 1 : 5 phase in sample A are obviously stronger than in sample B, which indicates that the relative content of the 1 : 5 phase is smaller in the ribbons with $z = 7.5$. According to the Scherrer method the 2 : 17 cell sizes of samples A and B are about 28 and 36 nm, respectively, which is similar to the report in [16]. Figure 2 shows the temperature dependence of the coercivity of samples A and B. The coercivity of sample A reduces with the temperature increase from RT to 200°C and then increases when the temperature is further increased from 200 to 500°C . The value of H_c is about 3.2 kOe at 500°C . Therefore, the abnormal temperature dependence of coercivity is obtained in sample A, indicative of the modern $\text{Sm}(\text{Co},\text{Fe},\text{Cu},\text{Zr})_z$ magnets. In contrast, the coercivity of sample B monotonously decreases with the temperature increase, which is similar to that in traditional $\text{Sm}(\text{Co},\text{Fe},\text{Cu},\text{Zr})_z$ magnets [17]. According to the experimental results [2–5, 7, 18], both types of magnets possess the same microstructure. The different behaviour of the temperature dependence of coercivity between A and B results from the composition discrepancy. It was verified experimentally that the abnormal temperature dependence of coercivity in modern $\text{Sm}(\text{Co},\text{Fe},\text{Cu},\text{Zr})_z$ magnets is closely related to the Cu content in the cell boundary phase [5, 18, 19]. With increasing Cu content in the cell boundary phase, the value of coercivity increases and the behaviour of the abnormal temperature dependence of coercivity disappears. Because the Sm content in sample B is less than that in sample A, there is relatively more content of the 1 : 5 cell boundary phase in sample A than that in sample B, as shown on the XRD patterns of samples A and B (figure 1). Therefore, more Cu content exists in the 1 : 5 cell boundary phase in sample B.

Figure 3 shows the MFM images with a scan size of $5 \mu\text{m} \times 5 \mu\text{m}$ for the two samples at room temperature. The

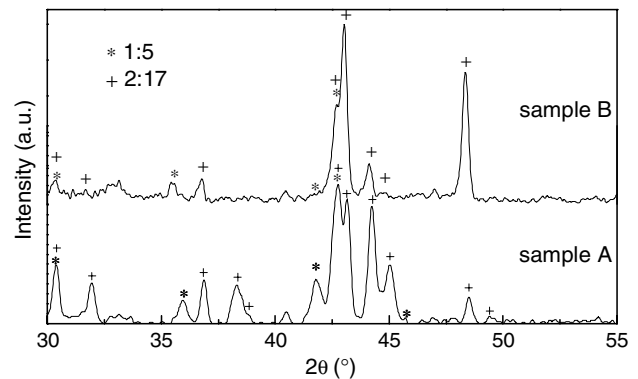


Figure 1. The XRD patterns of $\text{Sm}(\text{Co},\text{Fe},\text{Cu},\text{Zr})_z$ ribbons with $z = 7.0$ (A) and 7.5 (B).

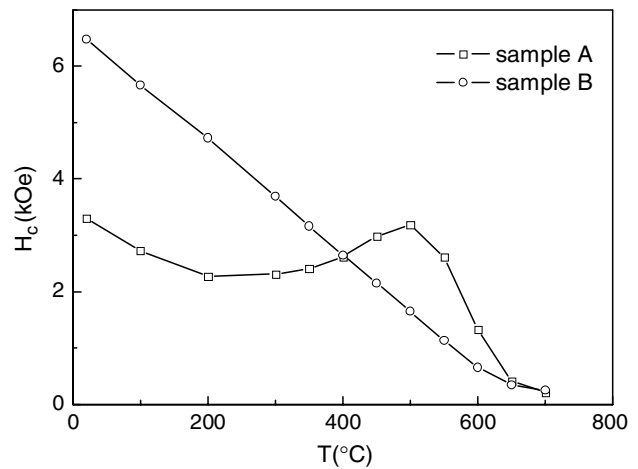


Figure 2. Temperature dependence of coercivity of $\text{Sm}(\text{Co}, \text{Fe}, \text{Cu}, \text{Zr})_z$ ribbons with $z = 7.0$ (A) and 7.5 (B).

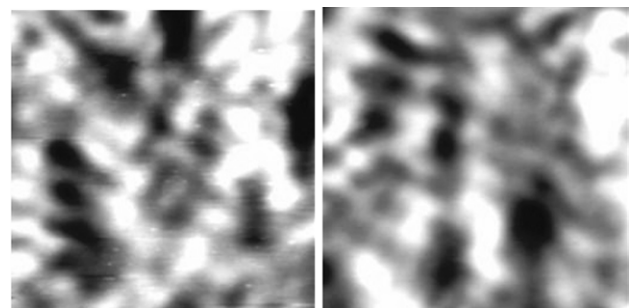


Figure 3. The MFM images with a scan size $5 \mu\text{m} \times 5 \mu\text{m}$ for samples with $z = 7.0$ (left) and 7.5 (right) at RT. The bright and dark areas (magnetic domains) are due to the magnetic moments out of the plane.

black and bright areas (about 500–700nm) contrast in the images, which result from the magnetic moments out of the plane, denote the domains with opposite magnetization, respectively. Obviously, the domains size of both A and B samples are much larger than their grains size according to the results of analysis by the Scherrer method from XRD. The magnetic structure is so called multigrain domains or interaction domains also found in other nanocrystalline PM ribbons and nanocomposite ribbons [7, 20, 21]. The interaction domains are considered as the result of exchange interactions

between the spins of adjacent grains. Unfortunately, the exchange coupling across grains cannot be identified in the MFM images. In fact, the 2 : 17 cells are insulated by the 1 : 5 cell boundary phase in $\text{Sm}(\text{Co},\text{Fe},\text{Cu},\text{Zr})_z$ magnets with a cellular structure. The experimental result of chemical analysis indicates that Cu is mostly concentrated at the 1 : 5 cell boundary [6]. Because Cu is nonmagnetic, both the exchanging constant and the magnetocrystalline anisotropy constant of the 1 : 5 phase in sample B are less than those in sample A. Consequently, it is expected that IGEC in sample A is stronger than that in sample B.

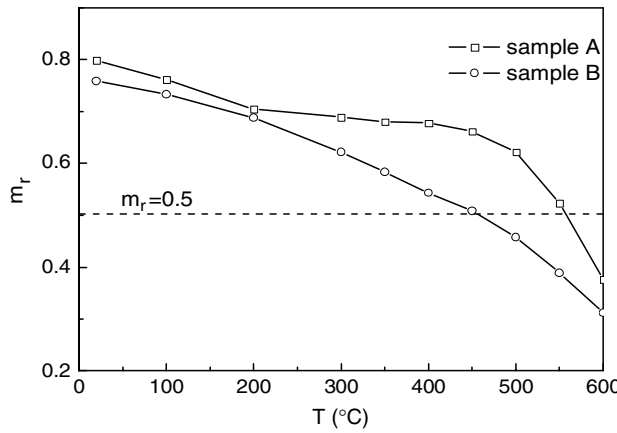


Figure 4. The temperature dependence of remanence ratio for two samples.

In order to compare the IGEC in sample A with that in sample B, the temperature dependence of the remanence ratio of samples A and B is shown in figure 4. $m_r = M_r/M_s > 0.5$, i.e. the remanence enhancement can be observed in both samples at $T \leqslant 450^\circ\text{C}$. In nanocrystalline PMs, the magnetic moment of a grain is parallel to that of the neighbouring grains through IGEC, resulting in the remanence enhancement [7,22]. Thus, a strong IGEC exists in both ribbons. Although the value of m_r decreases with temperature increase in both samples A and B, m_r of sample A shows a slower decrease rate, still being 0.62 at 500°C . The m_r of sample A is larger than that of sample B in the whole range of temperature, which is important to achieve a high temperature performance. Thus, it can be concluded that IGEC in modern $\text{Sm}(\text{Co},\text{Fe},\text{Cu},\text{Zr})_z$ magnets is stronger than that in traditional ones, especially in the high temperature range showing the abnormal coercivity increase.

Figure 5 shows the recoil loops of magnetization and demagnetization processes at RT and 500°C . The behaviour of magnetization and demagnetization curves for sample A is visibly different from that of sample B. In sample A, the processes of magnetization and demagnetization are almost irreversible at RT, but become relatively reversible at 500°C as shown in figure 5. In contrast, the sample B shows a high degree of reversibility in magnetization and demagnetization processes at both RT and high temperature. The difference in magnetization and demagnetization between A and B results from the characteristics of the 1 : 5 cell boundary phase. At RT, the cell boundary phase is magnetically softer than the cell phase in traditional $\text{Sm}(\text{Co},\text{Fe},\text{Cu},\text{Zr})_z$ magnets, which is

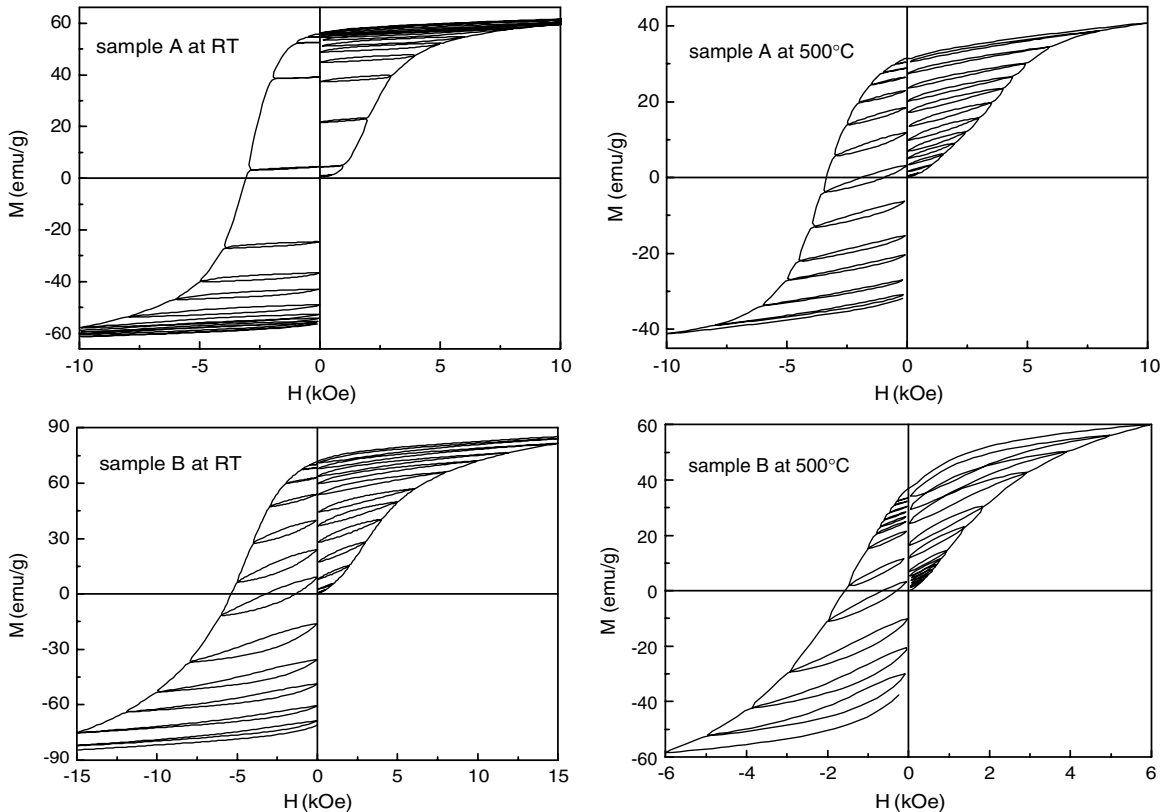


Figure 5. The recoil loops in the initial magnetization and demagnetization state, respectively, at RT and 500°C .

opposite to that in modern ones due to the Cu content in the cell boundary phase [6]. Thus, the reversal of the magnetic moments in cell boundary in sample B is easier than that of the 2 : 17 cell matrix, and these moments should turn back on the removal of the external field due to IGEC. Therefore, sample B shows a high degree of reversibility in its magnetization and demagnetization processes, which is similar to the behaviour of nanocomposite PMs [7, 13]. The same behaviour is observed for sample A at high temperatures, which indicates that the cell boundary phase becomes magnetically softer than the cell phase.

As shown in figure 5, the recoil loops do not close for both samples. According to the reports on nanocomposite PMs in [21, 23, 24], such a behaviour is attributed to the effect of the stray field on the irreversible behaviour of the soft phase when the cell boundary phase is considered to be magnetically soft. Recently, the coercivity mechanism was found to be controlled mainly by the pinning of domain walls in the modern $\text{Sm}(\text{Co},\text{Fe},\text{Cu},\text{Zr})_z$ PMs, but also in the traditional ones when the temperature is below the Curie temperature of the cell boundary phase. For the inhomogeneous domain-wall pinning, it is noticed that IGEC can also lead to the open recoil loops as shown in figure 5. In the cycle of a recoil loop, the exchange coupling brings about free energy for the neighbouring moments being parallel which is different from that for being antiparallel, and then the magnetic moments of the cell boundaries occur an irreversible process. In other words, both IGEC and stray field can lead to the open recoil loops in $\text{Sm}(\text{Co},\text{Fe},\text{Cu},\text{Zr})_z$ PMs. Unfortunately, we cannot judge which kind of interaction has a major contribution to the open recoil loops.

In a real system, the relation

$$\delta_m(H) = [J_d(H) - J_r(\infty) + 2J_r(H)]/J_r(\infty) \quad (1)$$

is used to estimate the intensity of the IGEC [25]. Here the remanent $J_r(H)$ can be obtained after applying and subsequent removal of a direct field H , $J_d(H)$ after saturation and the subsequent application and removal of a direct field H in the reverse direction, and $J_r(\infty)$ is the saturated remanent and denoted as J_r in the following for convenience. It is well known that the positive value of $\delta_m(H)$ is due to IGEC, while the negative value of $\delta_m(H)$ is the result of dipole–dipole coupling [21, 25–29]. Figure 6 shows δ_m versus H (Henkel plot) at different temperatures. At RT, strong IGEC exists in both ribbons because of the large positive value of δ_m . The maximum value of δ_m of sample A is higher than that of sample B at the same temperature. Therefore, IGEC in sample A is stronger than in sample B, which is consistent with the results shown in figure 4. With the increase in temperature, IGEC decreases due to the steep drop in the exchange constant, especially the exchange constant of the cell boundary phase. For sample B at 500 °C, the obtained negative values of δ_m indicate the strong effect of the stray field on the magnetization processes at high temperature.

In summary, the difference in the magnetic behaviour between the modern and traditional $\text{Sm}(\text{Co},\text{Fe},\text{Cu},\text{Zr})_z$ ribbons results from the variation of the structural characteristics in the cell boundary phase. Due to strong IGEC, the interaction domain is observed in nanocrystalline $\text{Sm}(\text{Co},\text{Fe},\text{Cu},\text{Zr})_z$ ribbons. Because of the large Cu content in the cell

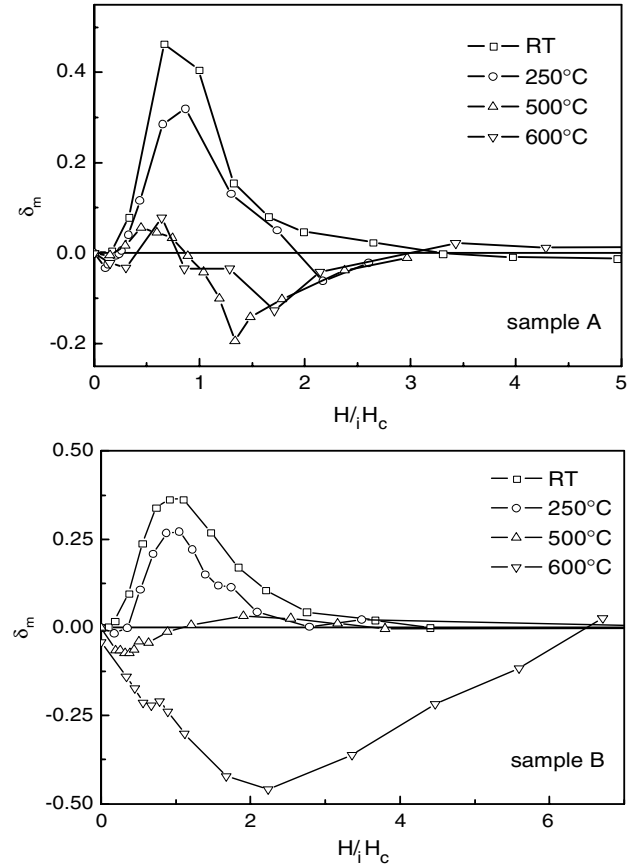


Figure 6. Henkel plot at various temperatures of samples with $z = 7.0$ (top) and $z = 7.5$ (bottom).

boundary phase in traditional $\text{Sm}(\text{Co},\text{Fe},\text{Cu},\text{Zr})_z$ ribbons, IGEC in modern $\text{Sm}(\text{Co},\text{Fe},\text{Cu},\text{Zr})_z$ ribbons is stronger. As a result, the remanence is higher in modern $\text{Sm}(\text{Co},\text{Fe},\text{Cu},\text{Zr})_z$ ribbons. Besides the stray field, IGEC can result in the open recoil loops for inhomogenous domain-wall pinning in $\text{Sm}(\text{Co},\text{Fe},\text{Cu},\text{Zr})_z$ PMs.

Acknowledgment

The work was supported by the National Natural Science Foundation of China.

References

- [1] Popov A G, Korolev A V and Shchegoleva N N 1990 *Phys. Met. Metallogr.* **69** 100
- [2] Goll D, Kleinschroth I, Sigle W and Kronmüller H 2000 *Appl. Phys. Lett.* **76** 1054
- [3] Zhou J, Skomski R, Chen C, Hadjipanayis G C and Sellmyer D J 2000 *Appl. Phys. Lett.* **77** 1514
- [4] Goll D, Kronmüller H and Stadelmaier H H 2004 *J. Appl. Phys.* **96** 6534
- [5] Liu J F, Chui T, Dimitrov D and Hadjipanayis G C 1998 *Appl. Phys. Lett.* **73** 3007
- [6] Hadjipanayis G C, Tang W, Zhang Y, Chui S T, Liu J F, Chen C and Kronmüller H 2000 *IEEE Trans. Magn.* **36** 3382
- [7] Hadjipanayis G C 1999 *J. Magn. Magn. Mater.* **200** 373
- [8] Gabay A M, Tang W, Zhang Y and Hadjipanayis G C 2001 *Appl. Phys. Lett.* **78** 1595
- [9] Skomski R 1997 *J. Appl. Phys.* **81** 5627

- [10] Gong W and Ma B M 1999 *J. Appl. Phys.* **85** 4657
- [11] Tang W, Zhang Y, Hadjipanayis G C and Kronmüller H 2000 *J. Appl. Phys.* **87** 5308
- [12] Chen C H, Gong W, Walmer M H, Liu S and Kuhl G E 2002 *J. Appl. Phys.* **91** 8483
- [13] Kneller E F and Hawig R 1991 *IEEE Trans. Magn.* **27** 3588
- [14] Skomski R and Coey J M D 1993 *Phys. Rev. B* **48** 15812
- [15] Chen Z M, Zhang Y, Ding Y Q, Hadjipanayis G C, Chen Q and Ma B M 1999 *J. Appl. Phys.* **85** 5908
- [16] Yan A, Bollero A, Müller K H and Gutfleisch O 2002 *Appl. Phys. Lett.* **80** 1243
- [17] Durst K-D, Kronmüller H and Ervens W 1988 *Phys. Status Solidi a* **108** 403
- [18] Liu S, Yang J, Doyle G, Potts G and Kuhl G E 2000 *J. Appl. Phys.* **87** 6728
- [19] Liu J F, Zhang Y, Dimitar D and Thomas G 1999 *J. Appl. Phys.* **85** 2800
- [20] Zhang H W, Sun Z G, Zhang S Y, Han B S, Shen B G, Tung I C and Chin T S 1999 *Phys. Rev. B* **60** 64
- [21] Zhang H W, Zhao T Y, Rong C B, Zhang S Y, Han B S and Shen B G 2003 *J. Magn. Magn. Mater.* **267** 224
- [22] Bauer J, Seeger M, Zern A and Kronmüller H 1996 *J. Appl. Phys.* **80** 1667
- [23] Zhang H W, Zhang S Y, Shen B G and Lin C 1999 *J. Appl. Phys.* **85** 4660
- [24] Goll D, Seeger M and Kronmüller H 1998 *J. Magn. Magn. Mater.* **185** 49
- [25] Kelly P E, O'Grady K, Mayo P I and Chantrell R W 1989 *IEEE Trans. Magn.* **25** 3881
- [26] Chen Q, Ma B M, Liu B, Huang M Q and Laughlin D E 1999 *J. Appl. Phys.* **85** 5917
- [27] Chiriac H, Marinescu M, Buschow K H J, de Boer F R and Bruck E 1999 *J. Magn. Magn. Mater.* **202** 22
- [28] Jin Z Q, Okumura H, Zhang Y, Wang H L, Munoz J S and Hadjipanayis G C 2002 *J. Magn. Magn. Mater.* **248** 216
- [29] Zhang H W, Rong C B, Du X B, Zhang J, Zhang S Y and Shen B G 2003 *Appl. Phys. Lett.* **82** 4098